Separation Science and Technology
Publication details, including instructions for authors and subscription information:
http://www.informaworld.com/smpp/title~content=t713708471

Analysis of the Variation of the Upper Discontinuity in Sedimentation Batch Test

R. Font; P. García; M. Pérez

To cite this Article Font, R. , García, P. and Pérez, M.(1998) 'Analysis of the Variation of the Upper Discontinuity in Sedimentation Batch Test', Separation Science and Technology, 33: 10, 1487 — 1510
To link to this Article: DOI: 10.1080/01496399808545062
URL: http://dx.doi.org/10.1080/01496399808545062

SEPARATION SCIENCE AND TECHNOLOGY, 33(10), pp. 1487–1510, 1998

Analysis of the Variation of the Upper Discontinuity in Sedimentation Batch Test

R. FONT* and P. GARCÍA
DEPARTAMENTO DE INGENIERÍA QUÍMICA

M. PÉREZ
DEPARTAMENTO DE INGENIERÍA DE SISTEMAS Y COMUNICACIONES

UNIVERSIDAD DE ALICANTE
APARTADO 99, ALICANTE, SPAIN

ABSTRACT

Variations of the supernatant-suspension discontinuity in batch sedimentation tests are examined using numerical simulation, considering the corresponding momentum laws for the noncompression zone and for the compression zone separately. A generalized treatment, considering some assumptions that are discussed, and introducing dimensionless variables is carried out. The paper analyses the variations of the derivative of the supernatant-suspension discontinuity height with respect to time versus the ratio of the supernatant-suspension discontinuity height to the initial supernatant-suspension discontinuity height. In cases where it is possible to estimate the location of the characteristic that rises from the bottom tangently to the sediment surface in a height–time diagram, the value of the critical solids concentration (boundary between hindered settling zone and compression zone) can be obtained. Another important contribution is the mathematical explanation of the exponential decrease of the sediment height versus time from the critical point (when the sediment curve joins with the upper discontinuity) to time infinity; this variation has been observed with many suspensions but has not been justified. This analysis is applied to two suspensions, considering their experimental data.

Key Words. Batch test; Sedimentation; Tory; Roberts

* To whom correspondence should be addressed.

INTRODUCTION

In the batch test of flocculated suspensions with low initial solids concentration, at least two discontinuities of solids concentration can be considered: a) the upper discontinuity or the supernatant-suspension discontinuity at the top of the suspension, and b) the sediment or compression zone interface that rises from the bottom of the cylinder. From the critical point when there is only sediment, Roberts observed that the descending upper discontinuity follows an exponential law (1). The solids frequently settle in the upper part (hindered settling zone), forming stable aggregates or flocs, whereas in the sediment or compression zone the solids form a network or matrix, with the displaced fluid flowing upward through the channels as stated by Fitch (2–4) who presented a very wide theory considering the momentum balance, the rising of the characteristics—lines of constant solids concentration in the hindered settling zone—, etc. Tiller (5) presented the first important analysis of the batch test which considered the two zones. Later Font (6, 7) widened some considerations by referring to the rise of the characteristics that emerge tangently from the sediment curve in a height–time diagram, and this fact was also tested by simulation of the batch test (8).

In Tory plots the data for the subsidence rate of the upper discontinuity in batch testing are plotted versus the height of suspension (9). A useful analysis of these plots was presented by Fitch (4). These plots are normally of interest when working with suspensions whose initial solids concentration is in the noncompression range. Tory plots are useful for obtaining data on the sedimentation rate in the noncompression range and are very important for determining the location of the critical points in accordance with the Roberts' method (1). In flocculated suspensions where the sediment discontinuity cannot readily be observed or measured, the rise of the sediment can be deduced by joining the critical points obtained from batch tests with the same initial solids concentration and different initial heights, as indicated by Fitch (3). With an estimate of the sediment curve, continuous thickeners can be designed by using results from batch tests (3, 4, 6, 7, 10). One aim of this paper is to explain the variations obtained with the Tory plots by simulation of the batch tests, and the application of these curves to obtain some important parameters such as the critical concentration (boundary between noncompression and compression ranges). In some cases, as commented upon in the last part of this paper, estimation of the settling flux density–solids concentration curve can be obtained.

GENERALIZED TREATMENT

Some basic relationships and dimensionless equations are considered in this section in order to present a generalized treatment. Figure 1 shows the evolution of the different zones and interfaces in a batch test. In this paper the volume fraction of solids is expressed as ϕ_s in the hindered settling range of concentration, from zero to the critical volume fraction of solids, and as ϵ_s from the critical volume fraction of solids ϵ_{s1} to the maximum value ϵ_{smax}. The volume fraction of solids depends on the distance x to the bottom of the cylinder and the time t. In order to consider the theory of sedimentation as presented elsewhere (2–8), the known material and momentum balances that can be applied to sedimentation batch tests are summarized in Table 1 for easy review.

- Equations (1) and (2) are the continuity balances.
- In the noncompression range, the sedimentation velocity of solids is determined by a balance of the gravitational force and the drag force. If the inertial effects due to acceleration of the particles are negligible, the sedimentation velocity $(-u_s)$ equals the terminal sedimentation velocity $(-u_{st})$ as indicated in Eq. (3) [values of the settling rate u_s $(= dx/dt)$ are negative in accordance with the positive semi-axis X considered in Fig. 1 and values of $(-u_s)$, therefore, are positive; throughout this paper all the negative magnitudes are converted to positive, writing them in parentheses and with a minus sign].

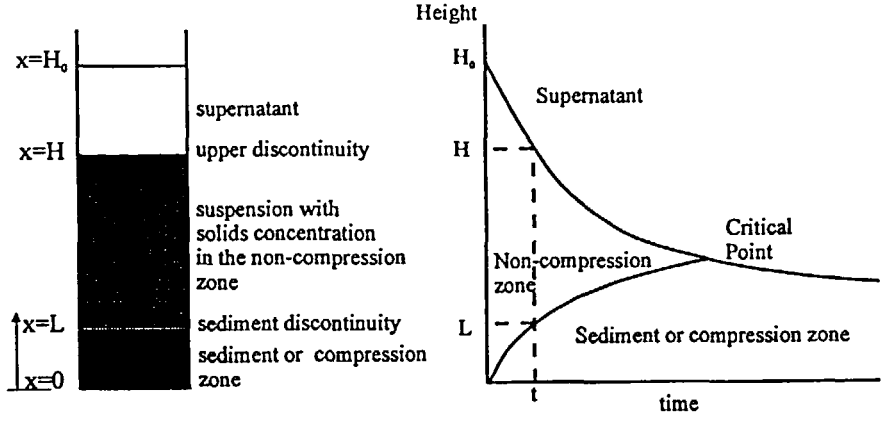

FIG. 1 Batch testing and evolution of discontinuities and zones.

TABLE 1
Material and Momentum Balances

	Noncompression zone, $0 < \phi_s < \epsilon_{s1}$	Compression zone, $\epsilon_{s1} < \epsilon_s < \epsilon_{smax}$
Continuity equation	$\frac{\partial \phi_s}{\partial t} - \frac{\partial[\phi_s(-u_s)]}{\partial x} = 0$ (1)	$\frac{\partial \epsilon_s}{\partial t} - \frac{\partial[\epsilon_s(-u_s)]}{\partial x} = 0$ (2)
Momentum equation	$-u_s (= -u_{st}) = f(\phi_s)$ (3)	$\frac{dp_s}{d\epsilon_s}\left[-\frac{\partial \epsilon_s}{\partial x}\right] = (\Delta\rho) g \epsilon_s - \frac{\mu}{k}(-u_s)$ (4)
Other relations	$-u_s = \frac{\Delta\rho g \phi_s k}{\mu}$ (5) $k_0^L = \lim_{\phi_s \to 0}(k\phi_s)$ (7) $= \frac{(-u_{so})\mu}{g\Delta\rho}$	$-u_{st} = \frac{\Delta\rho g \phi_s k}{\mu}$ (6) $p_s = f(\epsilon_s)$ (8) $k = f(\epsilon_s)$ (9)

- In the compression range the momentum balance, also neglecting the inertial effects, can be expressed as indicated in Eq. (4), where $\Delta\rho$ is the difference between the density of solids and the density of liquid, g is the positive value of acceleration due to gravity, and μ is the liquid viscosity (2, 5) (compressive stress = gravitational force − drag force).
- Equations (5) and (6) refer to the relation between the settling rate in the noncompression zone and the terminal settling rate in the absence of a solids pressure gradient and the permeability k in accordance with some definitions presented elsewhere (2).
- A parameter k_0^L is defined in Eq. (7).
- The relations between the effective pressure p_s and the permeability k in the compression range are indicated by Eqs. (8) and (9), respectively.

Table 2 indicates the assumptions considered in order to present a generalized case which is closely followed by many real systems. These assumptions are based on data obtained with two types of calcium carbonate suspensions (8, 11), where relations similar to those shown in Table 1 were obtained. No other systems with all the data indicated in Table 1 have been found in the literature. Nevertheless, as the variations of many batch tests are close to those presented in a generalized way in this paper (1, 4, 9), it can be deduced that the relations assumed are probably within the range including the data of many real systems. A generalized treatment was carried out instead of considering the calcium carbonate data in order to show that the conclusions obtained can be applied to many suspensions. Nevertheless, logical variations

of the physical properties must be assumed in order to obtain the simulated results.

For flocculated suspensions, the parameter AVI (average volume index), denoted in this paper by j, means the ratio of the total volume of an aggregate to the volume of solid inside the aggregate. The volume fraction of aggregates equals $j\epsilon_s$, and the interaggregate voidage occupied by free liquid equals $1 - j\epsilon_s$. The value ϵ_{s1} is the boundary volume fraction of solids between the noncompression range and the compression range when the aggregates touch each other, as in a fixed bed, while maintaining their identity. By considering that the porosity of a fixed bed of spheres (12) equals approximately 0.36, the total volume fraction of aggregates at the critical solids concentration is equal to 0.64, as indicated by Eq. (10).

With respect to the noncompression zone, the following statements are presented.

1. Equation (11) considers the variation of the settling velocity in accordance with the Richardson and Zaki (13) expression. On many occasions the variations of the settling rate to the power 4.65 vs the solids concentration are convex curves (12–14); this can be a consequence of a decrease of the parameter j or a decrease of the mass of solids in an aggregate. In a previous paper (8) it was deduced that this variation can be explained by assuming only a decrease of the parameter j with solids concentration

TABLE 2
Assumptions Considered

Noncompression zone, $0 < \phi_s < \epsilon_{s1}$	Limit	Compression zone, $\epsilon_{s1} < \epsilon_s < \epsilon_{smax}$
$-u_s = -u_{so}(1 - j\phi_s)^{4.65}$ (11)	$\epsilon_{s1} = \dfrac{0.64}{j_1}$ (10)	$\epsilon_{smax} = 2\epsilon_{s1}$ (15)
		$-u_{st} = \dfrac{6.4672 \times 10^{-5}(-u_{so})}{\epsilon_s j_0} \times (\{\mathrm{ATN}[-10(j_0\epsilon_s - 1.92)]\} + 90)$ (16)
$j = a - b\phi_s$: For $\phi_s = 0 \rightarrow a = j_0$ For $\phi_s = \epsilon_{s1} \rightarrow j = j_1 = j_0/2$ (12)		
$-u_s = -u_{so}\left(1 - 2j_1\phi_s + \dfrac{j_1^2\phi_s^2}{0.64}\right)$ (13)	$\epsilon_{s1} = \dfrac{1.28}{j_0}$ (14)	$\epsilon_s = \epsilon_{smax} - ((\epsilon_{smax} - \epsilon_{s1}) \exp(-p_s/p_A))$ (17)

as a consequence of the aggregates being closer at higher solids concentration than at lower solids concentration, and the liquid layer that surrounds the aggregate being thinner at high solids concentration than at low solids concentration.

2. Equation (12) considers a linear variation of j vs the volume fraction of solids. In addition, it is also assumed that the value of j at infinite dilution ($\phi_s = 0$) is twice the value of j at the critical solids concentration (ϵ_{s1}). These assumptions have been considered in accordance with the deviation of some experimental data from the Richardson and Zaki equation (8, 11, 14–16); i.e., the value j varies from 6 to 2 for calcium carbonate suspensions or from 1000 to 600 in some metal hydroxides suspensions. In other metal hydroxide suspensions the values of j and its variation is much less (around 70), but the form of the Tory plots is similar to those cases with great variation of j, indicating that this factor is not very important. From Eqs. (11) and (12), Relation (13) is obtained.
3. Taking into account that j_1 equals $j_0/2$, Relation (14) is deduced.

In the compression range, the following assumptions are considered.

1. The maximum concentration is twice the critical concentration (Eq. 15) assuming a considerable variation of solids concentration in the interval of effective solids pressure developed in batch tests. This occurs approximately with calcium carbonate suspensions (8, 11). For small variations of solids concentration in the sediment, the conclusions stated in this paper are also valid because the sediment height variation is small, as can be deduced after a complete reading of this paper. For great variations of the solids concentration inside the sediment, some conclusions could be different, as can also be deduced from this paper. Nevertheless, the variation assumed is rather great.
2. A variation of the terminal settling rate ($-u_{st}$) vs the volume fraction of solids ϵ_s indicated by Eq. (16), in which the following variation is assumed. At values of $j_0\epsilon_s$ between 1.28 and 1.8, the decrease of the settling flux density is small as a consequence of the formation of channels that favor the upward circulation of fluid between the matrix of solids. Between 1.8 and 2.2 there is a considerable decrease of ($-u_{st}$) as a consequence of the stretching of the matrix of solids (another interval could have been assumed). At $j_0\epsilon_s$ is greater than 2.2, values of ($-u_{st}$) are small (small permeability) because the channels are very thin (Fig. 2 shows the variation of the settling flux density after a change of variables indicated in the following paragraphs; the variation assumed is one of the possibilities). Note that the terminal settling rate ($-u_{st}$) in the compression range is the same when there is no compressive stress or

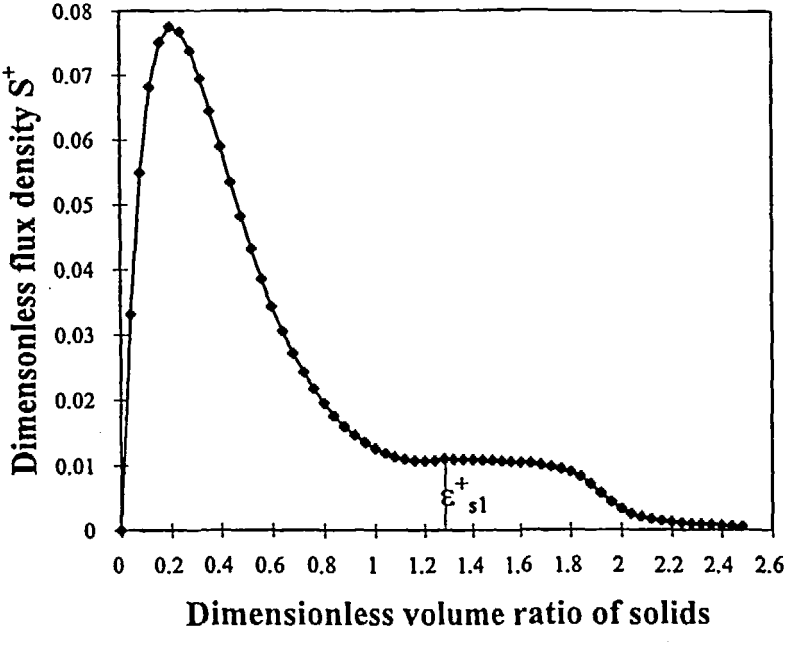

FIG. 2 Dimensionless settling flux density vs dimensionless volume ratio of solids.

no gradient of solids pressure and the inertial effects of acceleration or deceleration are logically negligible. This means that the terminal settling rate is the maximum settling rate of solids at the corresponding concentration in the most favorable conditions. Inside the compression zone, the real settling rate and the real settling flux density are less than the maximum values of the terminal settling rate and the settling flux density obtained from the permeability, and that corresponds (after corresponding changes of variables) to the portion of the curve shown in Fig. 2. The experimental data of the settling flux density variation vs concentration that can be obtained from the literature normally corresponds to the noncompression or hindered settling zone, and for many occasions the location of the critical concentration is not clear. By considering the variation that can be deduced from the permeability data of calcium carbonate suspensions (11) and other data published in the literature (17–23), the relation indicated by Eq. (16) has been assumed. The shape of the curve in Fig. 2 is logical based on some experimental data; nevertheless, it

must be emphasized that other variations could have been assumed, and although the simulated results would have been different, the general tendencies of the variations would probably be similar to those presented in this paper. (Note that the previous analysis is based on values of $j_0\epsilon_s$ that can be higher than 1 because the parameter j_0 can be much higher than 1.)

3. In Eq. (17) an exponential variation of ϵ_s vs the effective pressure p_s in agreement with the relation of Tiller and Khatib (24) is assumed. The experimental data obtained for the calcium carbonate suspension follows this relation which considers that the data from the maximum critical solids concentration is obtained in the low solids pressure range, corresponding only to sedimentation and not to filtration, permeation, or centrifugation (8).

As mentioned previously, although these assumptions are not applicable to all suspensions, in many batch tests the tendencies of the discontinuity heights to vary are similar to those presented in this paper.

Table 3 presents the corresponding dimensionless variables needed to present a generalized treatment, and Table 4 summarizes the balance equations and the relationships between the different variables using the dimensionless variables. Fig. 2 shows the variation of the dimensionless settling flux density S^+ vs the volume ratio of solids ϕ_s^+ or ϵ_s^+ for all intervals of solids concentrations. In the compression range the settling flux density refers to the terminal settling velocity (maximum value possible in the absence of a compressive stress).

SIMULATED RESULTS

In a previous paper (8) the method used for simulating batch testing was presented. This method distinguishes the noncompression zone from the compression zone in accordance with the equations previously presented.

TABLE 3
Definitions of Dimensionless Variables

$$N = \frac{p_A j_0^2}{\Delta\rho g (k_0^L)^{1/2}} \quad (18)$$

$$\phi_s^+ = j_0\phi_s \quad (19)$$

$$\epsilon_s^+ = j_0\epsilon_s \quad (20)$$

$$t^+ = \frac{j_0 (k_0^L)^{1/2}\Delta\rho g}{\mu N} t \quad (21)$$

$$x^+ = \frac{j_0}{(k_0^L)^{1/2} N} x \quad (22)$$

$$-u_s^+ = \frac{\mu}{k_0^L \Delta\rho g}(-u_s) \quad (23)$$

$$\epsilon_s^+ = j_0\epsilon_s \quad (24)$$

TABLE 4
Dimensionless Balance Equations

Noncompression zone, $0 < \phi_s^+ < 1.28$	Limit	Compression zone, $1.28 < \epsilon_s^+ < 2.56$
$\frac{\partial \epsilon_s^+}{\partial t^+} - \frac{\partial[\epsilon_s^+(-u_s^+)]}{\partial x^+} = 0$ (25)	$\epsilon_{s1}^+ = 1.28$ $\epsilon_{smax}^+ = 2.56$	$\frac{\partial \epsilon_s^+}{\partial t^+} - \frac{\partial[\epsilon_s^+(-u_s^+)]}{\partial x^+} = 0$ (26)
$-u_s^+ = \left(1 - \phi_s^+ + \frac{\phi_s^{+2}}{2.56}\right)^{4.65}$ (27)		$\frac{dp_s^+}{d\epsilon_s^+}\left[-\frac{\partial \epsilon_s^+}{\partial x^+}\right] = \epsilon_s^+ - \frac{\epsilon_s^{+2}}{B}(-u_s^+)$ (27)
		where $B = 6.3095 \times 10^{-5}(\{\text{ATN}[-10(\epsilon_s^+ - 1.92)]\} + 90)$ (28)
		$\epsilon_s^+ = 2.56 - 1.28 \exp(-p_s^+)$ (29)

Figure 3 shows the simulated results obtained for a batch test with an initial solids concentration ϕ_{so}^+ equal to 0.6. The variation of the supernatant-suspension discontinuity height, the sediment height, and the constant solids concentration lines are drawn versus time. Three zones can be distinguished in the suspension. Zone a, between the H-axis and the characteristic of ϕ_s^+ equal to 0.6 (line of constant solids concentration and constant settling rate) that arises from the bottom and that corresponds to the initial solids concentration; in this zone the concentration is constant and equals the initial one. Zone b, between the characteristic corresponding to the initial solids concentration and the characteristic that arises tangentially to the sediment from the bottom that corresponds to ϕ_s^+ equal to 0.86; all the characteristics in this zone arise from the bottom. Zone c, between the characteristic that arises tangentially to the sediment from the bottom and the sediment; in this zone the characteristics arise from the top of the sediment. Inside the sediment or the "compression zone," the lines of constant concentration are divergent up to the critical time. The intercept of the upper discontinuity and the sediment surface takes place at the critical point *C*. The intercept of the characteristic that arises tangentially to the sediment from the origin and separates Zone b from Zone c with the upper discontinuity is denoted point *D*.

Considering the points shown in Fig. 3, values of $-dH^+/dt^+$ at each point were determined by taking into account the point in question and the previous and later points presented in the graph. By correlating these three points to a parabolic equation, differentiating the function, and calculating the value

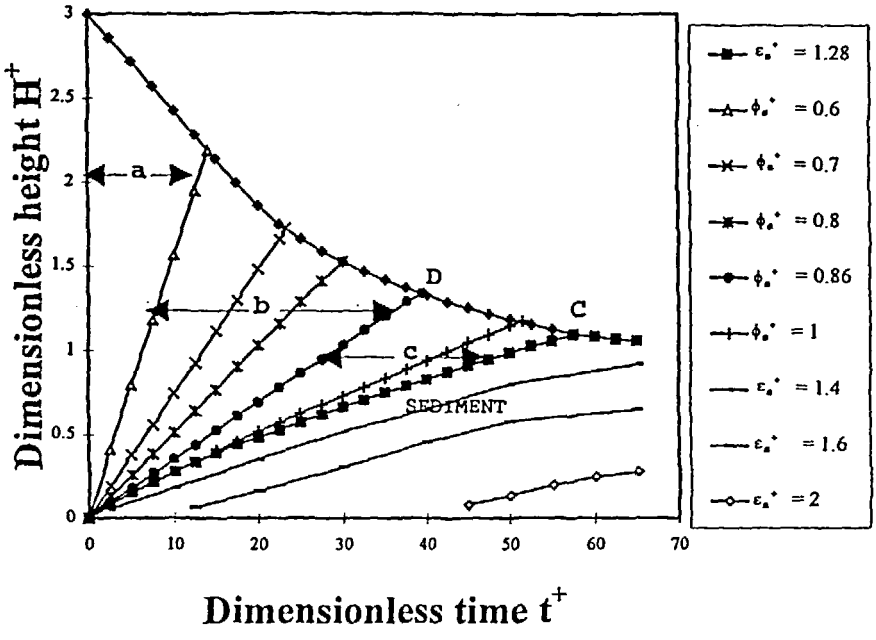

FIG. 3 Variation of zones and lines of constant concentration in a batch test with initial dimensionless volume fraction of solids $\phi_{s0}^{+} = 0.6$.

at the point considered, values of $-dH^{+}/dt^{+}$ were obtained. Figure 4 shows the corresponding values of $-dH^{+}/dt^{+}$ vs H^{+}/H_0^{+} (Tory plot), indicating the situations of point *C* (critical point) and point *D* (corresponding to the upper discontinuity height with separation of Zone b and Zone c, which coincides with the intercept of the upper discontinuity and the characteristic line that arises tangentially from the sediment at the bottom of the cylinder). Considering the variation of the subsidence rate $-dH^{+}/dt^{+}$ vs time, a linear variation on the bottom corresponding to the situation when all the suspension is sediment can be observed. There is a considerable variation above this linear variation due to the critical point (discontinuity), a short, nearly linear variation corresponding to Zone c, a great variation of $-dH^{+}/dt^{+}$ in Zone b, and a constant value of $-dH^{+}/dt^{+}$ in Zone a. Note that the small variation of $-dH^{+}/dt^{+}$ corresponding to Zone c is a consequence of the characteristics that arise tangentially from the sediment, and as the slope of the sediment curve varies slowly with time, the characteristics have a similar settling rate. This causes the presence of a quasi-linear variation of dH^{+}/dt^{+} between points *C* and *D*.

The location of point D in a batch test can be interesting because one way to estimate the critical concentration (boundary between the noncompression range and the compression range) is by the following equation:

$$\epsilon_{s1} = \frac{\phi_{so} H_0}{H_D} \tag{30}$$

that was deduced previously (8). Consider the dimensionless variables

$$\epsilon_{s1}^{+} = \frac{\phi_{so}^{+} H_0^{+}}{H_D^{+}} \tag{31}$$

Application of the previous equation to the data presented in Fig. 4 gives a value around 1.28 for ϵ_{s1}^{+}, which is the value considered in the simulation program. Nevertheless, the location of point D is only approximate.

Other, different Tory plots (subsidence rate of the upper discontinuity height vs height ratio) can be obtained, depending on the situation of the

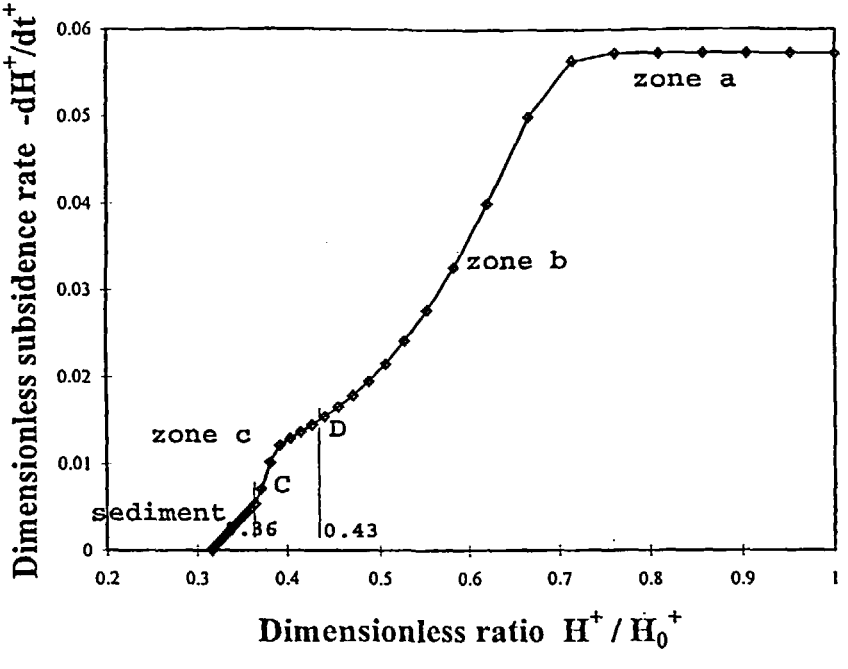

FIG. 4 Variation of the dimensionless subsidence rate of the upper interface $-dH^{+}/dt^{+}$ vs the height of the upper discontinuity/initial height of the upper discontinuity ratio H/H_0^{+} for the run with dimensionless volume fraction of solids $\phi_{so}^{+} = 0.6$ and dimensionless initial height of the upper discontinuity $H_{so}^{+} = 3$.

initial solids concentration in the S^+–ϕ_S^+ curve (Fig. 2). By considering the Fitch analysis of discontinuities (3), the remaining cases can be easily deduced. From the Tory plot it is also possible to deduce the location of the initial solids concentration in the S^+–ϕ_S^+ curve (Fig. 2).

The observation of points C and D depends mainly on the shape of the settling flux density–solids concentration curve. For batch tests where there is a great solids discontinuity above and under the sediment (which depends on the settling flux density–solids concentration curve), observation of points C and D will be clearer than for the opposite case.

ANALYSIS OF THE VARIATION OF $-dH/dt = f(H)$ FROM THE CRITICAL POINT. EXPLANATION OF ROBERTS' EXPERIMENTAL LAW

From Fig. 4 it can be observed that the variation of the settling rate versus the height of the upper discontinuity is nearly linear and in accordance with the empirical equation proposed by Roberts (1):

$$-dH/dt = K(H - H_\infty) \tag{32}$$

An explanation of this behavior is presented in this section. The continuity equation (Eq. 2) can be written as

$$\frac{\partial \epsilon_s}{\partial t} + u_s \frac{\partial \epsilon_s}{\partial x} = \epsilon_s \frac{\partial(-u_s)}{\partial x} = \epsilon_s^2 \frac{\partial(-u_s)}{\epsilon_s \partial x} \tag{33}$$

In the following equation, a coordinate space variable is introduced instead of the distance x. This variable is defined as

$$w = \int_0^x \epsilon_s dx \tag{34}$$

and consequently

$$dw = \epsilon_s dx \tag{35}$$

This coordinate space variable was also used by Shirato et al. (25, 26) when studying the behavior of suspensions in the compression range.

Coordinate space w defines the volume of solids per unit of cross section between the bottom of the cylinder and distance x.

The first term of Eq. (33) corresponds to the observed variation of ϵ_s with time, following the settling of the solids. Taking into account that at any time the solids above the layer settle with absolute velocity values less than that corresponding to the layer considered, and the opposite occurs with the solids under the layer considered, it can be deduced that the first term equals the

variation of ϵ_s vs time for a layer that has a constant amount of solids under it, and consequently the value of w is a constant. This analysis is based on the concept of substantial derivative presented in the literature. Then

$$\left(\frac{\partial \epsilon_s}{\partial t}\right)_w = \frac{\partial \epsilon_s}{\partial t} + u_s \left(\frac{\partial \epsilon_s}{\partial x}\right)_t \tag{36}$$

From Eqs. (33) and (36):

$$\frac{1}{\epsilon_s^2}\left(\frac{\partial \epsilon_s}{\partial t}\right)_w = -\left(\frac{\partial \frac{1}{\epsilon_s}}{\partial t}\right)_w = \left(\frac{\partial(-u_s)}{\partial w}\right)_t \tag{37}$$

This equation is similar to that obtained by other authors (25).

The momentum balance can be written as

$$\frac{dp_s}{d\epsilon_s}\left(-\frac{\partial \epsilon_s}{\partial x}\right)_t = \frac{dp_s}{d\epsilon_s}\left(-\epsilon_s \frac{\partial \epsilon_s}{\partial w}\right)_t = g\epsilon_s \Delta\rho - \frac{\mu}{k}(-u_s) \tag{38}$$

From the previous equation it can be deduced that

$$\begin{aligned}(-u_s) &= \left[\frac{k}{\mu} g\epsilon_s^2 \Delta\rho\right](1/\epsilon_s) - \left[\epsilon_s^3 \frac{dp_s}{d\epsilon_s}\frac{k}{\mu}\right]\left(\frac{\partial(1/\epsilon_s)}{\partial w}\right)_t \\ &= C_1(1/\epsilon_s) - C_2\left(\frac{\partial(1/\epsilon_s)}{\partial w}\right)_t\end{aligned} \tag{39}$$

where

$$C_1 = \frac{k}{\mu} g\epsilon_s^2 \Delta\rho \tag{40}$$

and

$$C_2 = \epsilon_s^3 \frac{dp_s}{d\epsilon_s}\frac{k}{\mu} \tag{41}$$

Introducing Eq. (39) into Eq. (37), the following can be written:

$$-\left(\frac{\partial(1/\epsilon_s)}{\partial t}\right)_w = \left(\frac{\partial(-u_s)}{\partial w}\right)_t = \left(\frac{\partial\left[(C_1(1/\epsilon_s)) - C_2\left(\frac{\partial(1/\epsilon_s)}{\partial w}\right)_t\right]}{\partial w}\right)_t \tag{42}$$

Parameters C_1 and C_2 depend on ϵ_S and consequently also depend on w and t. If C_1 and C_2 are constant or can be considered only a function of w, Roberts' law can be demonstrated as follows.

Applying Eq. (39) to an infinite time:

$$(-u_s)_{t=\infty} = 0 = C_1\left(\frac{1}{\epsilon_{s\infty}}\right) - C_2\left(\frac{\partial(1/\epsilon_{s\infty})}{\partial w}\right) \tag{43}$$

where $\epsilon_{s\infty}$ is the volume fraction of solids of each layer at infinity. As the solids concentration at infinity depends only on the buoyed weight of solids above the layer considered, $\epsilon_{s\infty}$ is a function of w.

Subtracting Eq. (43) from Eq. (39):

$$(-u_s) = C_1\left(\frac{1}{\epsilon_s} - \frac{1}{\epsilon_{s\infty}}\right) - C_2\left(\frac{\partial\left(\frac{1}{\epsilon_s} - \frac{1}{\epsilon_{s\infty}}\right)}{\partial w}\right)_t \tag{44}$$

Note that $\epsilon_{s\infty}$ depends on w. Introducing Eq. (44) in to the second term of Eq. (42) and considering that $\epsilon_{s\infty}$ does not depend on t:

$$-\left(\frac{\partial\left(\frac{1}{\epsilon_s} - \frac{1}{\epsilon_{s\infty}}\right)}{\partial t}\right)_w = \left(\frac{\partial\left[C_1\left(\frac{1}{\epsilon_s} - \frac{1}{\epsilon_{s\infty}}\right) - C_2\left(\frac{\partial\left(\frac{1}{\epsilon_s} - \frac{1}{\epsilon_{s\infty}}\right)}{\partial w}\right)_t\right]}{\partial w}\right)_t \tag{45}$$

The solution of Eq. (45) can be expressed as

$$\frac{1}{\epsilon_s} - \frac{1}{\epsilon_{s\infty}} = a\exp(-b(t - t_c)) \tag{46}$$

where t_c is the critical time, a is a function only of w, and b is a constant. The boundary condition at infinity is fulfilled in accordance with Eq. (44).

Applying Eq. (44) to the top of the sediment, where ϵ_s always equals ϵ_{s1} and consequently $\epsilon_{s\infty} = \epsilon_s = \epsilon_{s1}$, and w equals w_0, which is the maximum value corresponding to the whole suspension ($w_0 = \phi_{so}H_0$), it can be deduced that the velocity of the descending supernatant-sediment discontinuity u_0 is

$$(-u_0) = -\frac{dH}{dt} = M_0\exp(-b(t - t_c)) \tag{47}$$

where M_0 is the value corresponding to the preexponential factor for the maximum value of $w(w_0 = \phi_{so}H_0)$. Integrating Eq. (47) between (t, H) and (∞, H_∞):

$$\int_{H_\infty}^{H} dH = -\int_{\infty}^{t} M_0 \exp(-b(t - t_c))dt = H - H_\infty \tag{48}$$

$$= \frac{M_0}{b} \exp(-b(t - t_c))$$

From Eqs. (47) and (48):

$$-\frac{dH}{dt} = M_0 \frac{b}{M_0} (H - H_\infty) = b(H - H_\infty) \tag{49}$$

which coincides with Eq. (32), where K equals b.

Solution When C_1 and C_2 Depend on ϵ_s, and Consequently also Depend on w and t

In this case a system of differential equations must be considered to observe the variation of the upper interface. Using the dimensionless variables defined in Table 3, and also defining

$$dw^+ = \epsilon_s^+ dx^+ = j_0 \frac{j_0}{(k_0^L)^{1/2} N} \epsilon_s dx \tag{50}$$

Equation (42) can be written as

$$-\left(\frac{\partial(1/\epsilon_s^+)}{\partial t^+}\right)_{w^+} = \left(\frac{\partial \left[(C_1^+(1/\epsilon_s^+)) - C_2^+ \left(\frac{\partial(1/\epsilon_s^+)}{\partial w^+}\right)_{t^+}\right]}{\partial w^+}\right)_{t^+} \tag{51}$$

where

$$C_1^+ = B \tag{52}$$

and

$$C_2^+ = \epsilon_s^+ B \frac{dp_s^+}{d\epsilon_s^+} = B \frac{\epsilon_s^+}{2.56 - \epsilon_s^+} \tag{53}$$

Figures 5 and 6 show the variations of C_1^+ and C_2^+ vs w^+, respectively, for different values of t^+. These variations are deduced from the simulation program. It can be observed that there is movement of the variation curves in both cases.

For batch tests where the sediment heights after the critical point decrease to around or less than 20–30% of the height at the critical point, it is possible that the curves $C_1 = C_1(w, t)$ and $C_2 = C_2(w, t)$ for different times are close, and mean variations $C_1 = C_1(w)$ and $C_2 = C_2(w)$ can consequently

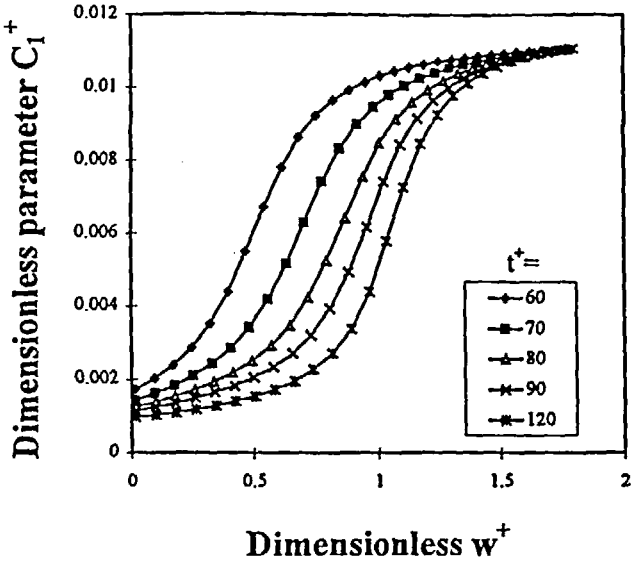

FIG. 5 Variation of the dimensionless parameter C_1^+ vs the dimensionless space coordinate w^+ for different dimensionless times t^+.

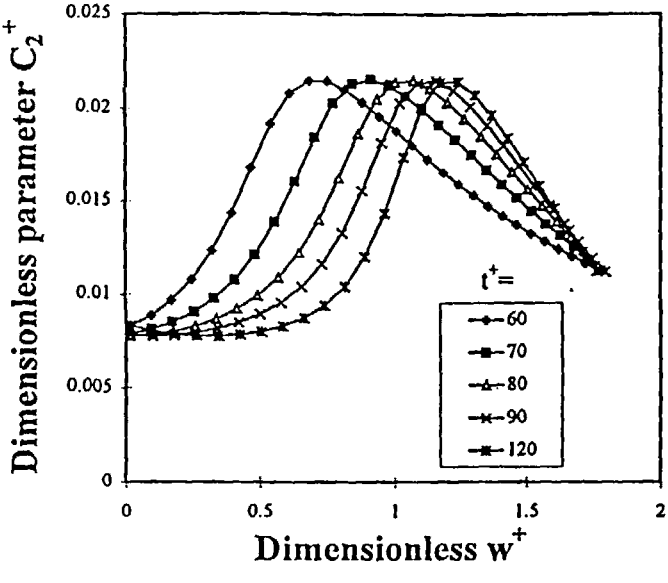

FIG. 6 Variation of the dimensionless parameter C_2^+ vs the dimensionless space coordinate w^+ for different dimensionless times t^+.

be roughly considered and independent of time, and the decreasing height of the sediment after the critical point can approximately follow the Roberts equation. Note also that the greatest variation of $-dH/dt$ takes place for the first period, when the curves $C_1 = C_1(w, t)$ and $C_2(w, t)$ are not very far apart. This is an explanation of the behavior observed in many suspensions in accordance with an analysis carried out by Fitch (4) concerning Tory plots, but there can be other cases where a deviation from the Roberts equation is clearly observed as a consequence of very great variations of $C_1(w)$ and $C_2(w)$ vs t or the fact that the hydrodynamics of the suspension does not follow the momentum balance considered as tested in many studies.

APPLICATION TO EXPERIMENTAL DATA

Figures 7 and 8 shows the experimental data corresponding to two suspensions, one of commercial calcium carbonate, whose experimental procedure has been presented elsewhere (11) and the other one of metal hydroxides, obtained from the precipitation of solutions with $NiSO_4 \cdot 6H_2O$, $ZnSO_4 \cdot 7H_2O$ and $CuSO_4 \cdot 5H_2O$ with $Ca(OH)_2$ (70 wt %) + $Mg(OH)_2$ (30 wt %) at a pH equal to 11.7. With both suspensions, it was possible to visually estimate the location of the sediment, because a considerable change of porosity could be observed. Nevertheless, the variations of the sediment are only used for testing the location of point D.

Figures 9 and 10 show Tory plots for both suspensions by the procedure explained with the simulated data previously presented. A similarity can be observed by comparing Fig. 4 with Fig. 9, with a nearly straight line corresponding to the sediment, a great change in the subsidence rate corresponding to the critical point, a slight variation corresponding to Zone c that ends in point D, the variation corresponding to Zone b, and the constant value of the subsidence rate corresponding to Zone a. Nevertheless, in Fig. 10, there is not a small variation in the subsidence rate above the critical point, indicating that Zone c is probably very small and the critical point C is close to point D.

Considering the locations of point D with both suspensions, the critical volume fractions of solids, calculated by Eq. (30), are 0.138 for the calcium carbonate suspension and 0.00905 for the metal hydroxide suspension. These practically coincide with those obtained from the intersection of the tangent to the sediment at the bottom with the supernatant-suspension discontinuity height.

In accordance with Eq. (10), and referring to the fact that the volume fraction of aggregates equals 0.64 at the critical solids concentration, the values of the average volume index (AVI) are 4.71 for the calcium carbonate suspension and around 70 for the metal hydroxide suspension. If these AVI

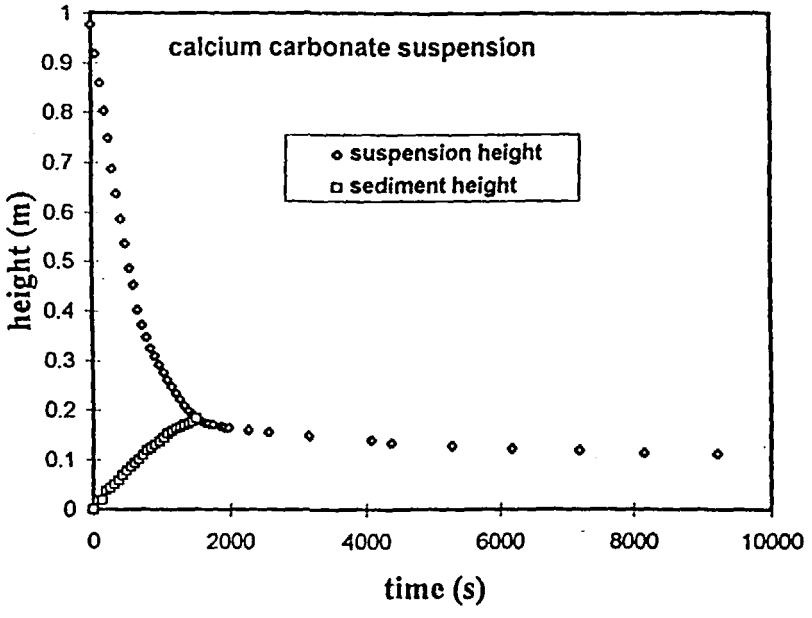

FIG. 7 Batch test of a calcium carbonate suspension (ϕ_{so} = 0.04239; H_0 = 0.977 m).

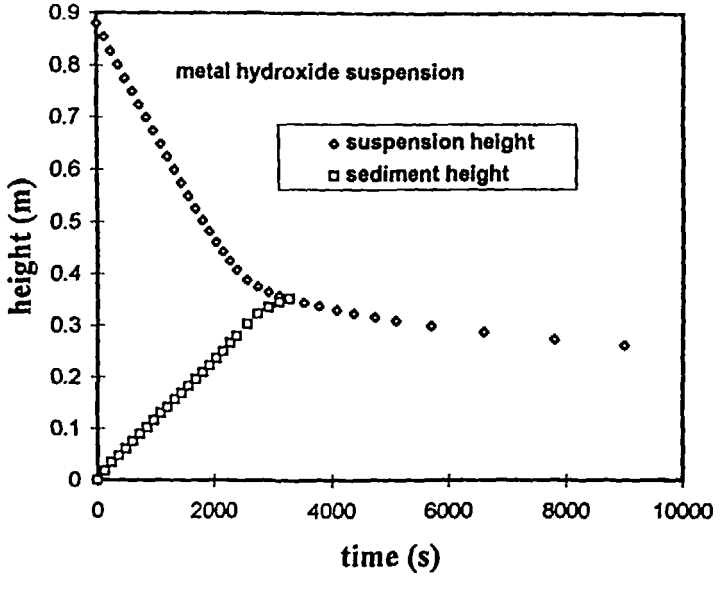

FIG. 8 Batch test of a metal hydroxide suspension (ϕ_{so} = 0.003806; H_0 = 0.88 m).

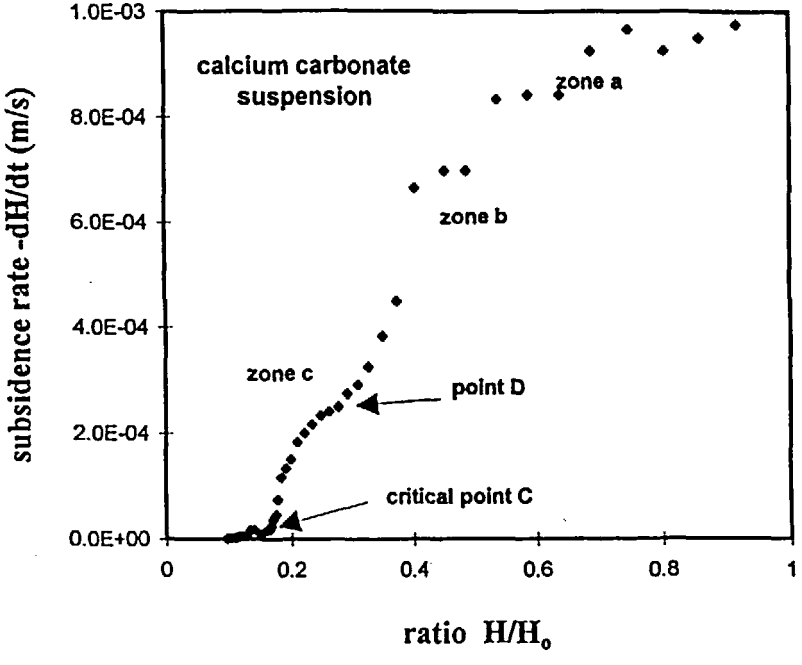

FIG. 9 Variation of the subsidence rate of the upper interface vs the height of the upper discontinuity/initial height of the upper discontinuity ratio H/H_0 for the run carried out with the calcium carbonate suspension ($\phi_{so} = 0.04239$; $H_0 = 0.977$ m; $H_D = 0.300$ m).

values or j remain constant, and considering Eq. (11) and the settling rate $(-u_{si})$ at the initial solids concentration ϕ_{si}, the settling flux density can be calculated as

$$S = \phi_s(-u_{so})(1 - j\phi_s)^{4.65} = \phi_s(-u_{si})\frac{(1 - j\phi_s)^{4.65}}{(1 - j\phi_{si})^{4.65}} \qquad (54)$$

Figures 11 and 12 show the estimated variations of the settling flux density versus the volume fraction of solids for both suspension, comparing these values with those obtained from direct determination in batch tests and/or determination considering the tangents to the upper discontinuity and characteristics drawn from the bottom or from the sediment considering the Kynch theory and its modification to compressible suspensions (6, 7). It can be observed that for the metal hydroxide suspension the estimated S is very close to the points determined by another independent method, whereas for the

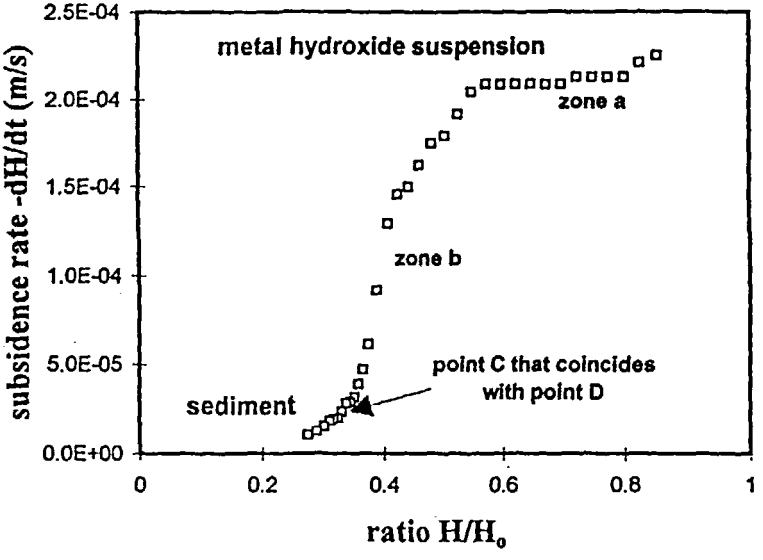

FIG. 10 Variation of the subsidence rate of the upper interface vs the height of the upper discontinuity/initial height of the upper discontinuity ratio H/H_0 for the run carried out with the metal hydroxide suspension (ϕ_{so} = 0.003806; H_0 = 0.88 m; H_D = 0.37 m).

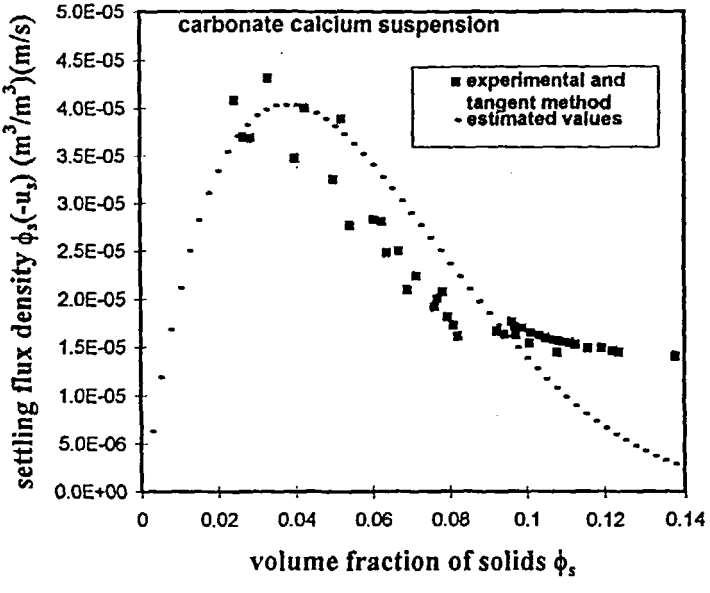

FIG. 11 Settling flux density vs volume fraction of solids: comparison for the calcium carbonate suspension.

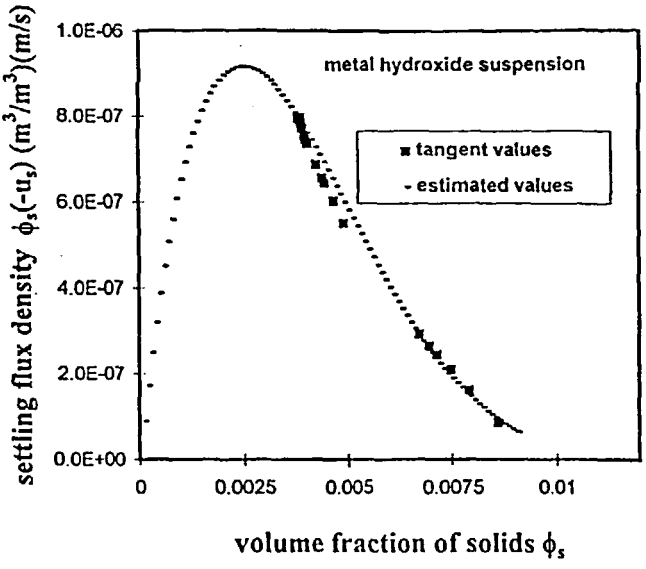

FIG. 12 Settling flux density vs volume fraction of solids: comparison for the metal hydroxide suspension.

calcium carbonate suspension, although the estimated variation is in the range of the experimental values, the shape is different. This different behavior can be explained by considering that the aggregates drag a small outer layer of fluid which can be very thin at high solids concentration. For aggregates with a small AVI value, as occurs with calcium carbonate suspensions, a small decrease of the outer layer of fluid causes a great decrease in the AVI value, and consequently this value cannot be considered constant. In the opposite case, when the AVI value is very high, a small decrease in the outer layer of fluid cannot significantly affect the AVI value as occurs with the metal hydroxide suspension. In any case, it must be emphasized that this method of estimating the settling flux density–solids concentration curve must be considered as an approximate method that must be compared with other alternatives.

CONCLUSIONS

The zones that can be distinguished in a batch test are equivalent to portions of curves found by plotting the derivative of the supernatant-suspension discontinuity height with respect to time versus the ratio of the supernatant-suspension discontinuity height to the initial supernatant-suspension disconti-

nuity height: constant settling rate, large decrease in the settling rate, slow decrease—nearly linear—in the settling rate, discontinuity in the settling rate corresponding to the critical point, and nearly linear variation in the sediment. It has been shown that by considering the point between the portion of the curve of a large decrease and a small decrease, which corresponds to the intercept of the upper discontinuity with the characteristic that arises from the bottom tangentially to the sediment curve, it is possible to estimate the critical solids concentration, the boundary value between the noncompression range and the compression range. In some cases the settling flux density-solids concentration variation can be estimated from the value of the critical solids concentration.

A mathematical explanation of the variation corresponding to the sediment height versus time after the critical point, which follows the exponential law observed in many suspensions, is presented.

SYMBOLS

ATN	arc tg or tg^{-1}
AVI	average volume index. Ratio between volume of aggregate or floc and solids volume (equals j) (dimensionless)
a	function of w given by Eq. (46) (dimensionless)
B	parameter in Eq. (28) (dimensionless)
b	parameter of Eq. (46) (dimensionless)
C	critical point in batch testing (intercept of the upper discontinuity and the sediment discontinuity)
C_1	parameter defined in Eq. (40) (dimensionless)
C_2	parameter defined in Eq. (41) (dimensionless)
C_1^+	parameter defined in Eq. (52) (dimensionless)
C_2^+	parameter defined in Eq. (53) (dimensionless)
D	intercept point of the characteristic that arises from the bottom tangentially to the sediment and the upper discontinuity
g	gravity acceleration (m/s^2)
H	height of the supernatant-suspension discontinuity (upper discontinuity) (m)
H_0	initial height of suspension at $t = 0$ (m)
H_∞	height of the suspension (sediment) at time-infinity (m)
H_D	height of point D (height of the intersection between the characteristic line arising from the bottom tangentially to the sediment curve and the upper discontinuity)
H^+	dimensionless height of the supernatant-suspension discontinuity (upper discontinuity) that equals $j_0 H/((k_0^L)^{1/2} N)$ in accordance with Eq. (22)

H_0^+ dimensionless initial height of suspension.
H_∞^+ dimensionless height of the suspension (sediment) at time = infinity
H_D^+ dimensionless height of point D
j AVI = average volume index. Ratio between volume of aggregate or floc and solids volume (dimensionless)
j_1 value of j at the critical volume fraction of solids ϵ_{s1} (dimensionless)
j_0 value of j at the initial solids concentration (dimensionless)
K parameter defined in Eq. (32) (s^{-1})
k permeability (m^2)
k_0^L parameter defined by Eq. (7) (m^2)
L_1^+ dimensionless sediment height
M_0 preexponential factor in Eq. (47)
N dimensionless parameter defined by Eq. (18)
p_A parameter in Eq. (17)
p_s effective pressure (N/m^2)
p_s^+ dimensionless effective pressure
S settling flux density [(m^3 solids/total m^3) × (m/s)]
S^+ dimensionless flux density [$=\phi_s(-u_s^+)$ or $\epsilon_s^+(-u_s^+)$]
t time (s)
t_c critical time (s)
t^+ dimensionless time
μ_0 velocity of the upper discontinuity (m/s)
u_s settling velocity of solids (m/s)
u_{si} initial settling velocity of solids (m/s)
u_{so} settling velocity of solids at infinite dilution (m/s)
u_{st} terminal settling rate (m/s)
u_{st}^+ dimensionless terminal settling rate
u_s^+ dimensionless settling rate
w volume of solids from the bottom per unit of cross section (m)
w^+ dimensionless volume of solids from the bottom per unit cross section
x distance down column (m)
x^+ dimensionless distance down column

Greek Letters

ϵ_s volume fraction of solids in sediment
ϵ_s^+ dimensionless volume ratio of solids that equals $j_0\epsilon_s$
ϵ_{s1}^* interaggregate porosity at volume fraction of solids ϵ_{s1}
ϵ_{s1} value of ϵ_s at cake surface (limit value between noncompression and compression zone)
ϵ_{smax} maximum value of ϵ_s in accordance with Eq. (17)
$\epsilon_{s\infty}$ value of volume fraction of solids that any layer reaches at time infinity (depending on w)

$\Delta\rho$ difference between the solids density and the fluid density (kg/m^3)
μ viscosity of fluid [kg/(m·s)]
ϕ_s volume fraction of solids in suspension
ϕ_{s_0} initial volume fraction of solids in suspension
ϕ_s^+ dimensionless ratio fraction of solids in suspension (equals $j_0\phi_s$)
$\phi_{s_0}^+$ initial dimensionless ratio fraction of solids in suspension (equals $j_0\phi_{so}$)

REFERENCES

1. E. J. Roberts, *Min. Eng.*, *1*, 61 (1949).
2. B. Fitch, *AIChE J.*, *25*(6), 913 (1979).
3. B. Fitch, *Ibid.*, *29*(6), 940 (1983).
4. B. Fitch, *Ibid.*, *39*(1), 27 (1993).
5. F. M. Tiller, *Ibid.*, *27*(5), 823 (1981).
6. R. Font, *Ibid.*, *34*(2), 229 (1988).
7. R. Font, *Ibid.*, *36*(1), 3 (1990).
8. R. Font, *Chem. Eng. Sci.*, *46*(10), 2473 (1991).
9. E. M. Tory, "Batch and Continuous Thickening of Slurries," Ph.D. Thesis, Purdue University, 1961.
10. W. P. Talmage and E. B. Fitch, *Ind. Eng. Chem.*, *47*(1), 38 (1955).
11. R. Font, M. Perez, and C. Pastor, *Ind. Eng. Chem. Res.*, *33*(11), 2859 (1994).
12. P. T. E. Shannon, E. Stroupe, and E. M. Tory, *Ind. Eng. Chem. Fundam.*, *2*, 203 (1963).
13. J. F. Richardson and W. N. Zaki, *Trans. Inst. Chem. Eng.*, *32*, 35 (1954).
14. W. R. Knocke, *J. Water Pollut. Control Fed.*, *58*(6), 784 (1986).
15. R. V. Stephenson, J. M. Montgomery, and E. R. Baumann, *Part. Sci. Technol.*, *4*, 237 (1986).
16. R. Font, A. F. Marcilla, and C. Zoffmann, *Powder Technol.*, *71*, 217 (1992).
17. E. M. Tory and P. T. Shannon, *Ind. Eng. Chem. Fundam.*, *4*, 194 (1965).
18. K. J. Scott, *Ind. Eng. Chem. Fundam.*, *7*, 484 (1968).
19. K. J. Scott, *Ibid.*, *7*, 422 (1970).
20. C. A. Petty, *Chem. Eng. Sci.*, *30*, 1451 (1975).
21. J. S. Turner and D. Glasser, *Ind. Eng. Chem. Fundam.*, *15*, 23 (1976).
22. K. P. Galvin and A. G. Waters, *Powder Technol.*, *53*, 113 (1987).
23. B. Fitch, *AIChE J.*, *36*(10), 1545 (1990).
24. F. M. Tiller and Z. Khatib, *J. Colloid Interface Sci.*, *100*(1), 55 (1984).
25. M. Shirato, H. Kato, K. Kobayashi, and H. Sakarazi, *J. Chem. Eng. Jpn.*, *3*, 98 (1970).
26. M. Shirato, T. Aragaki, A. Manabe, and N. Takeuchi, *AIChE J.*, *25*, 855 (1979).

Received by editor August 21, 1997
Revision received November 1997